Research Article | Vol. 29, No. 22 / 25 Oct 2021 / Optics Express 35161

Optics EXPRESS

Harvesting electrical energy using plasmon-enhanced light pressure in a platinum cut cone

HA YOUNG LEE,[1] MIN SUB KWAK,[1] KYUNG-WON LIM,[2] HYUNG SOO AHN,[1] GEON-TAE HWANG,[3] DONG HAN HA,[4] ROBERT. A. TAYLOR,[5] AND SAM NYUNG YI[1,6,*]

[1]*Department of Electronic Materials Engineering, Korea Maritime and Ocean University, Busan, 49112, Republic of Korea*
[2]*Korea Institute of Materials Science (KIMS), Changwon, Gyeongnam, 51808, Republic of Korea*
[3]*Department of Materials Science and Engineering, Pukyong National University, Busan, 48513, Republic of Korea*
[4]*Materials and Convergence Measurement Institute, Korea Research Institute of Standards and Science, Daejeon, 34113, Republic of Korea*
[5]*Department of Physics, University of Oxford, Parks Road, Oxford OX1 3PU, United Kingdom*
[6]*Interdisciplinary Major of Maritime AI Convergence, Korea Maritime and Ocean University, Busan, 49112, Republic of Korea*
[*]*snyi@kmou.ac.kr*

Abstract: We have designed a method of harvesting electrical energy using plasmon-enhanced light pressure. A device was fabricated as a cut cone structure that optimizes light collection so that the weak incident light pressure can be sufficiently enhanced inside the cut cone to generate electrical energy. An increase in the device's current output is a strong indication that the pressure of incident light has been enhanced by the surface plasmons on a platinum layer inside the cut cone. The electrical energy harvested in a few minutes by irradiating pulsed laser light on a single micro device was possible to illuminate a blue LED.

1. Introduction

Sunlight is one of the most important 'green' renewable energy sources, as it is ubiquitous. Solar cells, which convert light energy into electrical energy through the photovoltaic effect, are the most common way in which we harvest energy from light [1,2]. A less common use of light as an energy source is light pressure, which refers to the pressure on the surface of an object when light hits that object. To date, the practical uses of light pressure are optical tweezers and solar sails. Optical tweezers trap and manipulate micro or nano objects by using strong light pressure formed by a highly focused laser beam or in a "hot spot", a very small space where the electromagnetic (EM) field is tremendously enhanced by surface plasmon resonances [3–11]. Meanwhile, a solar sail (Light Sail 2), launched by "The Planetary Society", is now flying through space propelled only by the force of light particles emitted by the sun [12]. The solar sail works efficiently because there is no air resistance in outer space [13–15].

A small amount of energy can be harvested by using piezoelectric materials to convert vibrational energy into electrical energy. At this time, there are various methods of applying vibration energy. For example, X. Wang et al., obtained 0.15 nA and 0.7 mV output by vibrating a zigzag Pt electrode on a silver ZnO nanorod using ultrasonic waves [16], Y. Qi et al., produced PZT in the form of a nanoribbon and pulled it left and right to obtain an output of ~2.5 $\mu A/mm^2$ [17]. Human motion, sound waves, and wind can give force to piezoelectric materials and the resulting energy can power a variety of devices such as LEDs, nanosensors, and flexible devices [18–28]. Researchers' interest in piezoelectric materials has increased over the past decade due

#438337 https://doi.org/10.1364/OE.438337
Journal © 2021 Received 20 Jul 2021; revised 23 Sep 2021; accepted 24 Sep 2021; published 13 Oct 2021
Corrected: 25 October 2021

Optics EXPRESS

to their various applications in sensors and wearable or implantable devices [29–33]. Light pressure can also exert mechanical stress on piezoelectric materials. However, natural light pressure of approximately 4.5×10^{-6} N/m^2 on the Earth's surface is so weak that, until now, it has not been possible to produce enough electrical energy to operate electronics by irradiating the piezoelectric devices with natural light.

Meanwhile, surface plasmons (SPs) are a phenomenon in which electrons on a metal surface collectively vibrate due to an electric field being applied to a conductive metal interfacing with a dielectric. There are two types of surface plasmons: extended surface plasmons (ESPs) and localized surface plasmons (LSPs), and the coupling between them produces ultrahigh local optical field enhancement [34,35]. ESPs are confined to the vicinity of the interface between a metal and a dielectric medium and can propagate along the metal surface. ESPs can also be excited on metal surfaces with periodic structures or random roughness which provide additional momentum to photons to match the momentum of the SPs [36,37]. On the other hand, LSPs are excited on metal nanostructures smaller than the wavelength of the incident light as a result of the coherent interaction between the oscillating electric field and the conduction electrons [35,38,39]. For structures where metal nanostructures are present on a metal surface, both ESPs and LSPs can be excited by incident light. ESPs, propagating along a metal surface, form an enhanced evanescent EM field near the metal surface. The intensity, $|E|^2$, of the strong EM field formed by LSPs on the metal nanostructure surface sustaining ESPs can be further enhanced by the coupling of LSPs and ESPs [35]. As examples, M. Abutoama et al., studied ultrahigh electromagnetic field enhancement using silver grating [40,41] and described the ESPs-LSPs coupling process at Au nano-bipyramids on the Ag thin film geometry [42]. And W. Liang et al., presented the SERS response for the multiplex plasmonic arrays and observed an enhanced photocurrent response attributed by LSPs [43].

The simplest way to achieve enhanced EM fields is to irradiate light on the cut cone structure. This advantage of EM field enhancement makes it very useful for piezoelectric energy harvesting applications. For instance, it might be able to generate electrical energy to power the IoT-gas sensor, -temperature sensor or –bluetooth beacon with integration of an energy harvester. This method is expected to be an alternative to other energy harvesting technologies which use wind, sound, heat, friction, and magnetic fields as energy sources [16,28,44–47]. For this purpose, we have fabricated a light pressure electric generator (hereafter LPEG) with a unique cut cone structure, where the incident light reflects multiple times and resonates with SPs inside the cut cone, thereby maximizing the optical pressure exerted on the surfaces of the devices. First, we made an open cut cone structure by wet-chemically etching a GaAs (100) wafer. Metal, piezoelectric material, and a second layer of metal were deposited sequentially on the inside of the cut cone. We obtained an average current of 3.2 μA and a voltage of 200 mV by irradiating pulsed laser light of 401 nm wavelength and 11.1 mW power into an LPEG with a PZT layer between platinum (Pt) layers. In this experiment we used PZT and BNKT as piezoelectric materials. PZT is an inorganic compound in which lead (Pb), zirconium (Zr), titanium (Ti), and oxygen (O) are combined, and has the chemical formula $Pb(Zr_x\ Ti_{1-x})O_3$. As a ceramic perovskite material, it exhibits a piezoelectric effect in which a potential difference is formed by the polarization difference when pressure is applied. PZT is the most commonly used piezoelectric ceramic because of its higher sensitivity and operating temperature than other piezoelectric ceramics. And another piezoelectric material, BNKT is an inorganic compound in which bismuth (Bi), sodium (Na), potassium (K), titanium (Ti), and oxygen (O) are combined and has the formula $Bi_{1/2}(Na_{0.78}K_{0.22})_{1/2}TiO_3$. Although BNKT has low piezoelectric properties (d_{33}, pC/N), it is harmless to the human body because it does not contain lead, so many studies of BNKT are currently being conducted. Our result was to illuminate a blue light emitting diode (LED) with the harvested electrical energy after charging for 6 min using 30 capacitors connected in series. We have therefore demonstrated that it is possible to harvest electrical energy from plasmon-enhanced

Optics EXPRESS

light pressure to operate electronic devices by using a unique cut cone structure and piezoelectric material.

2. Fabrication

Figure 1 shows a schematic illustration of the fabrication process for the LPEG. The following is a detailed description of the process: (i) A circular pattern with a diameter of 50 μm was formed on a GaAs (100) wafer capped with 300 nm-thick SiO_2 using photolithography. The photoresist (GXR-601) and the SiO_2 layer were sequentially removed using acetone and a buffered oxide etchant, so only the GaAs region corresponding to the cut cone was exposed. (ii) Then, the thickness of the wafer was adjusted to 150 μm by lapping it in order to control the size of the cut cone. (iii) The lapped wafer was pasted onto a glass and etched in a solution of H_2SO_4: H_2O_2: H_2O = 1: 5: 5 for 2 h at room temperature, and during this process a cut cone was formed [48]. (iv) The bottom electrode of Pt/Ti (100 nm/10 nm) was deposited by e-beam evaporation. (v) A PZT layer was coated on the bottom electrode as follows; a commercial PZT solution of 0.4 mole was spin coated at 3000 rpm for 45 s, followed by pyrolysis processes on a hot plate at 250 °C for 5 min and 300 °C for 3 min in the air. An appropriate output is produced by setting the thickness of the PZT to at least 400 nm. Since the piezoelectric properties are generally stronger as the thickness of the piezoelectric material increases, the PZT layer coating process was repeated four times to avoid the layer being too thin. The PZT layer then underwent rapid thermal annealing at 650 °C for 5 min in a nitrogen atmosphere. (vi) Finally, the top electrode of Pt (100 nm) was deposited on the PZT layer by e-beam evaporation. The coating process of the BNKT layer was the same as that of the PZT layer, except that the pyrolysis was performed sequentially in air at 350 °C for 5 min and at 400 °C for 10 min. The details of the process are shown in Fig. S1 of Supplement 1.

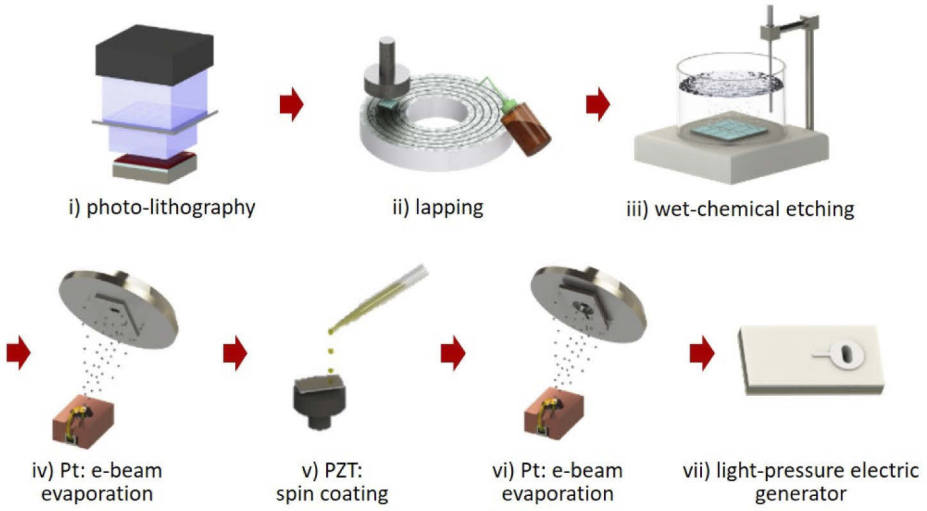

Fig. 1. Illustration of the fabrication process for the LPEG.

3. Details of the LPEG

In this experiment, we concentrated on the study of a structure capable of focusing light as efficiently as possible, to see if electricity could be generated by plasmon-enhanced light pressure. We chose a cut cone structure as the most efficient way to collect light. Figure 2(a) shows a schematic diagram of the concept of an LPEG device which harvests electric energy whenever

Optics EXPRESS

light is irradiated. The roughness increases the localized surface plasmon intensity, which in turn generates electricity. The device has a structure in which top Pt electrode/piezoelectric material/Pt/Ti/ layers are deposited one by one on the cut cone region with both the top and bottom open. Platinum covering the inside of cut cone simultaneously acts as the electrode and enables surface plasmon formation. The laser light acts on the Pt nanostructures inside the cut cone, generating a plasmon-enhanced optical force to deform the PZT [Fig. 2(b)].

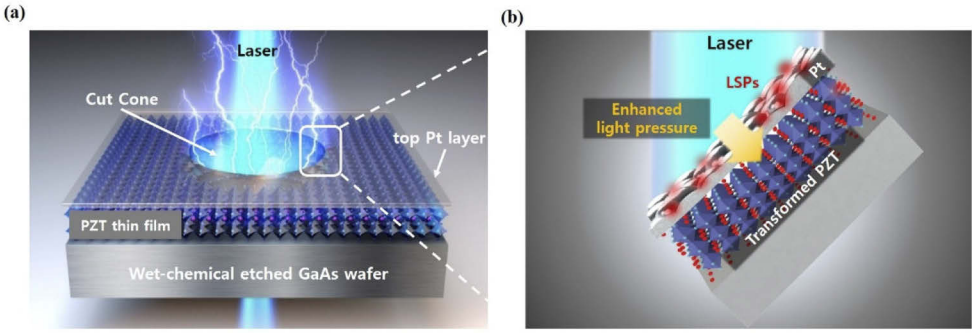

Fig. 2. (a, b) Schematic diagrams show the concept of energy output from a deformed perovskite structure that increases the intensity of light passing into the cut cone and the intensity of localized surface plasmons (LSPs) increased by surface roughness inside the cut cone.

Figure 3(a) depicts a cut cone made by wet-chemical etching a single GaAs (100) wafer. The cut cone was open at both top and bottom. The cut cones used in the fabrication of the sample were elliptical cut cones with a bottom slit width of 20 - 35 μm, obtained by etching a GaAs (100) wafer with a thickness of 150 μm as described earlier. Figure 3(b) is a cross-sectional FE-SEM image obtained following the vertical cutting of the cut cone region and it clearly shows the top and bottom of the cut cone open. Figures 3(c) and (d) are planar FE-SEM images taken in the early stages of making the bottom opening. In most cases, the top of the cut cone was a wide angled elliptical shape, but the bottom was a long, narrow slit. The inner surface of all cut cones comprised two large crystal planes and two small ones, due to the anisotropic etching rate. Cut cones with circular shape tops were rarely obtained while the bottom slits were consistently narrow and long, as shown in Fig. 3(d). The shape and size of the cut cone depend on the wafer surface index and thickness, mixing ratio of the etching solution, the etching time, and the shape of photo mask pattern [48]. We also fabricated cut cones in the same way using Si (100) substrates, but their inner surfaces consisted of four symmetrical (111) crystal planes, with both the top and bottom of each cut cone forming a square opening [49]. In this case, the above Pt electrode layers and the beneath PZT layer were electrically shorted along the boundaries between the crystal planes, so we could not use it as an LPEG device (Fig. S2 of Supplement 1). FE-SEM images in Figs. 3(e), (f), (g), and (h) were observed after depositing the top Pt electrode. Figures 3(e) and (f) show the thickness of the PZT layer increasing towards the base of the cut cone, being approximately 400 nm thick at its upper part but approximately 900 nm at its lower part. The inner surface of the cut cone was significantly different from the surface of the flat region outside the cut cone as shown in Figs. 3(g) and (h). In the flat region outside the cut cone, the surface Pt layer featured irregular shaped discs with a diameter of 100 – 300 nm, in a tight configuration without pores. On the other hand, the surface Pt layer inside the cut cone wall mostly consisted of ball-shaped grains and pores measuring less than 100 nm in width. These numerous nanograins can also acts as “hot spots”, where the electric field is greatly enhanced by SPs [50]. We presume that the unique structure of the cut cone with its slanted walls and open slit at its base help to give the Pt layer its grained and pored nanoscale roughness. It

Optics EXPRESS

appears that the nanoscale surface roughness of the cut cone wall causes multiple reflections of the incident light inside the cut cone, and also excites SPs on the top Pt layer, which results in the great enhancement of the EM field in the vicinity of the top layer.

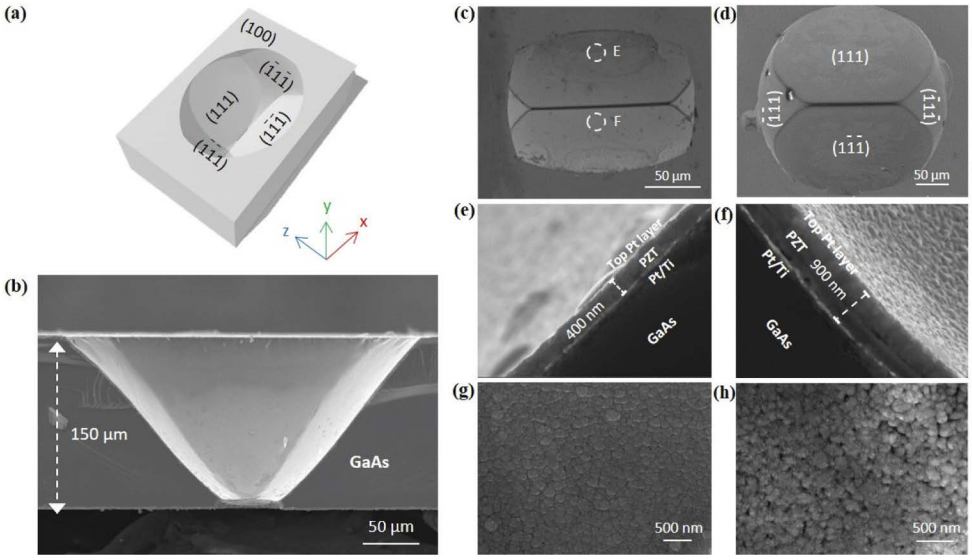

Fig. 3. (a) Three-dimensional illustration of the wet-chemical-etched GaAs in the form of a cut cone shaped microvoid structure with a slit at the bottom and surface indices. (b) Cross-sectional FE-SEM image of etched GaAs. (c, d) Planar FE-SEM images of cut cones. Cross-sectional images of (e), point E and (f), point F shown in (c), respectively, showing a PZT layer between two Pt layers. (g) Flat surface Pt layer outside the cut cone. (h) Grained and pored nano-roughness of surface Pt layer along the cut cone wall.

4. Conversion of plasmon-enhanced light pressure into the electrical energy

The LPEG generated current pulses, when it was irradiated by pulsed laser light, and the average pulse duration time of the current pulse was approximately 0.10 s when rotating the optical chopper at 72 rpm (Visualization 1). A photograph and a schematic of the measurement procedure are shown in Figs. 4(a) and (b), respectively. For the irradiation with laser light at a wavelength of 401 nm and power of 11.1 mW, a PZT-based LPEG generated an average current of approximately 3.2 μA, as shown in Fig. 4(c), and the charge amplifier gave 25 pC in Figs. 4(e) and (f). We also fabricated another kind of LPEG, in which lead-free BNKT was used as the piezoelectric material between Pt electrodes, as shown in Fig. 4(d). The output current of a BNKT-based LPEG was reduced noticeably to 1 μA when compared to that of a PZT-based LPEG, due to the smaller piezoelectric coefficient d_{33} of the BNKT layer compared to that of the PZT layer (Fig. S3 of Supplement 1). The response of our piezoelectric devices with cut cone structure to light irradiation was prompt and accurate, enabling current pulses to be generated immediately whenever laser light was irradiated on them.

As a control experiment, the device shown in Fig. 4(g) was used, where the piezoelectric layer was replaced with an insulating SiO_2 layer, which generated no current. As another control experiment, we also prepared a device with a Pt/PZT/Pt structure on a flat GaAs (100) substrate, as shown in Fig. 4(h). The top Pt surface of the device was the same as that shown in Fig. 3(g). In other words, there were no nanoscale grains or pores on the surface, so we did not expect any enhancement of the EM field due to the SPs by visible light. No current was generated by this device either when it was illuminated by laser light. From the results of Fig. 4, we see that in

Optics EXPRESS

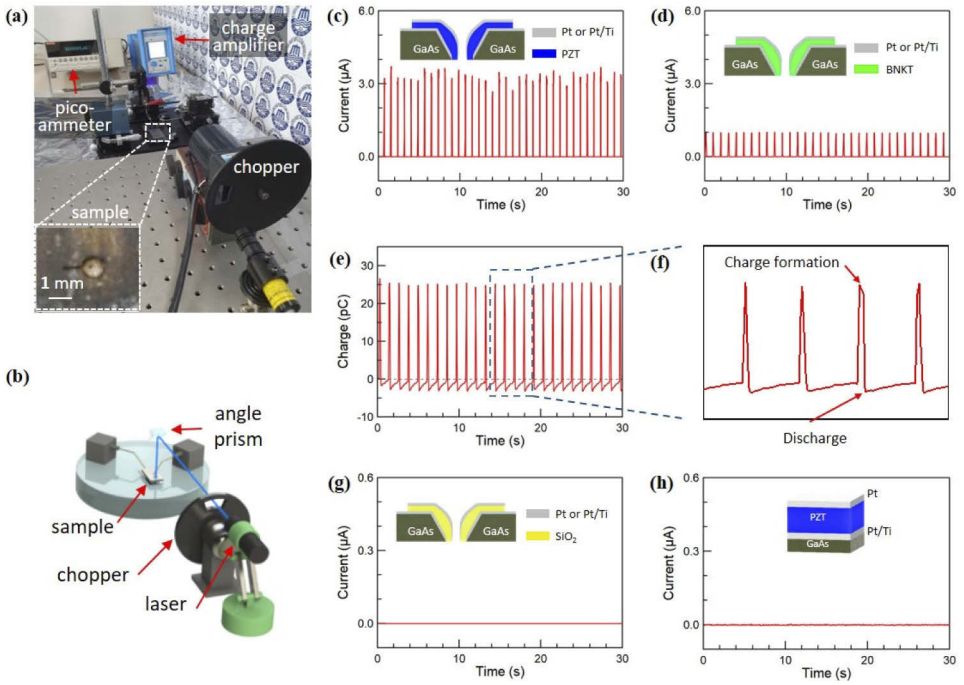

Fig. 4. (a) Experimental setup for measuring the electrical output of an LPEG, following irradiation by pulsed laser light. Inset of (a) is an optical image of a sample placed on a micro-stage. (b) Schematic diagram of the measuring system. Insets of (c), (d), (g) and (h) show the structure of each device. (c, d, g) The devices have the same cut cone structure, but the materials between Pt electrodes differ as (c) PZT, (d) BNKT, and (g) SiO_2. (e, f) The behavior of charge formation and discharge at PZT layer. (h) A PZT device fabricated on a flat GaAs (100) substrate. While rotating the optical chopper at 72 rpm, laser light at a wavelength of 401 nm and power of 11.1 mW was used to irradiate each device.

a structure with a Pt cut cone with a hot spot surface, current was generated in both PZT and BNKT (which have piezoelectric properties), but not in SiO_2. In addition, a device made of PZT, but without a cut cone structure, shows no current generation because it cannot collect light efficiently and no multiple reflection of the incident light is possible. Therefore, we propose that the light pressure was enhanced by SPs inside the unique cut cone structure with its nanoscale surface roughness as shown in Fig. 3(h). Here, the light pressure P, is given by

$$P = 2I/c = E^2/c^2\mu_0, \tag{1}$$

where I is the intensity of impinging light, c is the velocity of light, E is the electric field, and μ_0 is the permeability of free space. For 1.4 W/cm^2 laser intensity with 11.1 mW power and beam diameter of 1 mm, P = 4.65 × 10^{-5} N/m^2 (about 10 times the magnitude of natural solar pressure on the Earth's surface), and is too weak to generate any piezoelectric current in a device with a flat structure.

In order to confirm the enhancement of light pressure inside the cut cone by SPs, we measured the dependence of output current from the LPEG according to the surface power density of the light source and its wavelength measured in W/cm^2. The results are summarized in Figs. 5(a) and (b). For light of 401 nm, 531 nm, and 651 nm wavelengths, covering most of the visible light range, the output current was linearly proportional to the average surface power density of each pulse of incident light. We noted that the output current of an LPEG per unit of light

Optics EXPRESS

energy was greatest at 401 nm, and this reduced gradually as the incident wavelength increased. Moreover, all data points converged into a single straight line for normalized laser intensity, and this indicated that the output current was predominantly determined by the incident laser intensity. We performed the experiment again to observe the light pressure corresponding to the minimum current (Fig. S4 of Supplement 1). When the laser intensity was reduced to 0.4% (light pressure 0.0188×10^{-5} N/m^2), a current of up to ~ 15 nA could be observed. This result indirectly shows that the device's sensitivity is very high and that light is amplified very strongly in the cut cone structure. We monitored the temperature of the sample, which was stable within ± 0.2 °C during measurement, confirming that the pyroelectric effect was negligible. The random surface roughness acts as a coupler that matches the momentum of the photon and ESP. Thus, EM field amplitude near the surface can be enhanced greatly due to the excitation of ESPs by visible light and impart a force in the direction of propagation [36,37]. Especially, inhomogeneities in the electric field intensity due to presence of plasmonic nanostructures on the metal surface provide high field intensities. This phenomenon has been experimentally identified in surface enhanced Raman scattering [51]. LSPs, confined to metal nanostructures smaller than the wavelength of the incident light, also result in an intense EM field in the vicinity of the nanostructures. Moreover, it is reported that the EM field intensity, $\propto |E|^2$, in the vicinity of nanostructures on a metal layer sustaining ESPs can be enhanced by as much as 10^5 to 10^6 times by the coupling of LSPs and ESPs [34,35]. We believe that the intensity of the EM field was also enhanced greatly in the vicinity of the top Pt layer of the LPEG, due to the numerous Pt nanograins and pores on its surface. In addition, we believe that the intensity of the EM field was further increased by the incident light being reflected multiple times inside the cut cone. The resonant frequency of LSPs depends on the size, shape and arrangement of the nanostructures and dielectric environment [52]. Langhammer et al. found a general trend that the extinction peak maxima of novel metal nanoparticles in air, where the maximum of surface plasmon field occurs, were redshifted as the size of the nanoparticles increased [53]. More specifically, for Pt discs with a diameter of 76 nm, 120 nm, and 140 nm, they reported that the extinction peak maxima appeared at around 400 nm, 500 nm, and 600 nm, respectively. The results of Langhammer et al. are consistent with our results; the output current of an LPEG with a top Pt layer on the cut cone wall consisting mostly of grains less than 100 nm in size was greatest at 401 nm and decreased with increases to the incident wavelength. In addition, Raman spectra measurements were performed to confirm the difference in the surface plasmon intensity between the flat and cut cone (Fig. S5 of Supplement 1). As a result, the Raman intensity in the cut cone was about 4.16 times greater than that of the flat at 1001 cm^{-1}. This means that the surface enhanced Raman scattering phenomenon is stronger in the cut cone. FDTD (finite domain time difference) and COMSOL multiphysics simulation, a numeric calculation method, were performed to supplement the analysis on the generation of plasmon and the deformation of PZT through the results of electric field, stress, and electrostatic potentials on the roughened surface. The results in Fig. S6 of Supplement 1 are the distribution plots for the increased electric field for the surface with and without roughness. The electric field distribution of increased intensity can be seen between the nanosize particles. Meanwhile, the COMSOL simulation results for the stress and electrostatic potentials difference distributions formed in the PZT due to the increased electric field strength are shown in Figs. S7 and S8 of Supplement 1, respectively. If there is roughness on the surface, it can be seen that the stress and potential in the PZT are significantly increased. Through this analysis, it can be suggested that the increased electric field strength, that is, the light pressure, can deform the PZT and form a potential difference. Figure 5 and Fig. S5 ~ S8 of Supplement 1 strongly support the premise that the intensity of EM field or light pressure exerted on the LPEG was enhanced by SPs, thereby enabling devices to generate electric current.

We were able to illuminate an LED with the harvested electrical energy, thereby demonstrating that the LPEG is capable of producing electrical energy from light pressure to operate electronics.

Optics EXPRESS

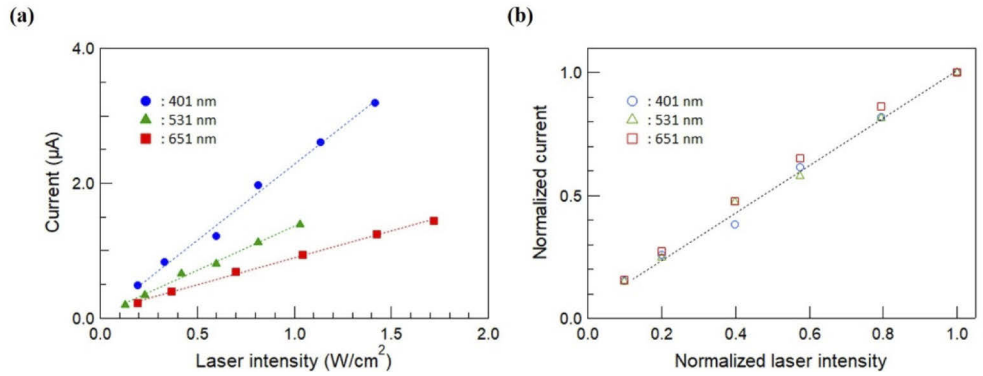

Fig. 5. (a, b) Changes in the device output current with variation in laser intensity and normalized laser intensity for three different wavelengths. The laser intensity of incident light on the device was controlled by using a neutral density filter.

Figure 6(a) shows that a voltage of 0.19 V was obtained after charging 30 capacitors connected in series (total 3 mF and 5.7 V) for 6 min using a PZT-based LPEG. Figures 6(b) and (c) clearly show we succeeded in illuminating the blue LED with the harvested electrical energy. Thus, we present the experimental observation of a mechanism to transform enhanced light pressure into electric power using plasmonic nanostructures.

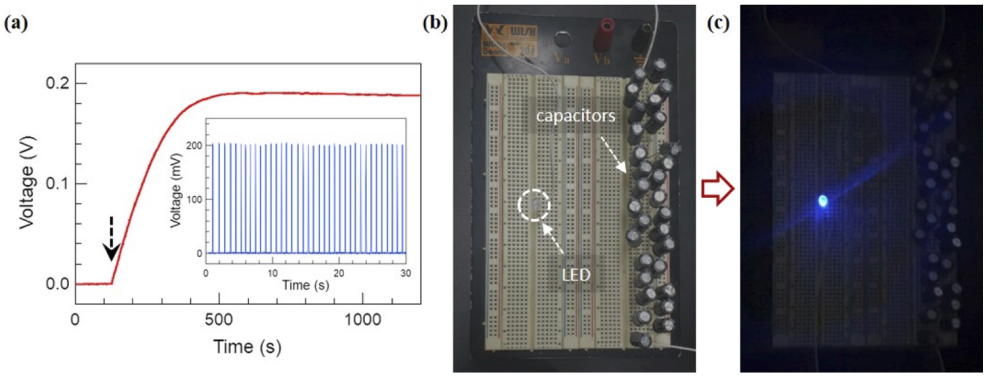

Fig. 6. (a) Charging of 30 capacitors connected in series (total 3 mF) with electrical energy harvested by a PZT-based LPEG. A dotted arrow indicates when charging started. Inset shows the output voltage for the irradiation of laser light of 401 nm and 1.4 W/cm^2. (b, c) Photographs show before and after the illumination of a blue LED with harvested electrical energy, respectively.

5. Conclusions

We have developed novel microscale piezoelectric devices which convert plasmon-enhanced light pressure into electrical energy. The devices, fabricated using GaAs (100) substrates, were designed with metal/piezoelectric material/metal layers on unique cut cone structures, which allowed weak incident light pressure to be sufficiently enhanced inside the cut cone for the generation of electrical energy. More specifically, SPs excited on the top Pt layer with its numerous nanograins and pores significantly enhanced the EM field in the vicinity of the layer. The dependence of the device's electrical output on the power and wavelength of the incident

Optics EXPRESS

light strongly supports the evidence that the enhancement of the EM field inside the cut cone was caused by SPs. The conversion of plasmon-enhanced light pressure into electrical energy confirms not only for a PZT-based device, but also for a device using an alternative piezoelectric material, BNKT. Our results demonstrate we could turn on a blue LED with the electrical energy harvested by irradiating the sample with a laser light on a single cut cone structure. Thus, this platinum cut cone structure is a promising candidate for generating current by plasmon-enhanced light pressure. Optimization of the size, number, and shape of cut cone structures will likely increase future output, making this structure potentially very useful. In particular, an LPEG using this mechanism could power wireless sensors and portable electronics as a new class of self-powering technologies that harvests electricity from the environment.

Funding. National Research Foundation of Korea (2017R1A2B4009832).

Acknowledgments. S. N. Yi thanks financial support from the Basic Science Research Program through the National Research Foundation of Korea (NRF) for help identifying collaborators for this work.

Disclosures. The authors declare no conflicts of interest.

Data Availability. Data underlying the results presented in this paper are not publicly available at this time but may be obtained from the authors upon reasonable request.

Supplemental document. See Supplement 1 for supporting content.

References

1. D. E. Carson and C. R. Wronski, "Amorphous silicon solar cell," Appl. Phys. Lett. **28**(11), 671–673 (1976).
2. J. You, L. Dou, K. Yoshimura, T. Kato, K. Ohya, T. Moriarty, K. Emery, C. -C. Chen, J. Gao, G. Li, and Y. Yang, "A polymer tandem solar cell with 10.6% power conversion efficiency," Nat. Commun. **4**(1), 1446 (2013).
3. A. Ashkin, J. M. Mziedzic, and T. Yamane, "Optical trapping and manipulation of single cells using infrared laser beams," Nature **330**(6150), 769–771 (1987).
4. A. Ashkin and J. M. Dziedzic, "Optical trapping and manipulation of viruses and bacteria," Science **235**(4795), 1517–1520 (1987).
5. M. L. Juan, M. Righini, and R. Quidant, "Plasmon nano-optical tweezers," Nat. Photonics **5**(6), 349–356 (2011).
6. A. Ashkin, J. M. Dziedzic, J. E. Bjokholm, and S. Chu, "Observation of a single-beam gradient force optical trap for dielectric particles," Opt. Lett. **11**(5), 288–290 (1986).
7. K. Svoboda, C. F. Schmidt, and B. J. Schnapp, "Direct observation of kinesin stepping by optical trapping interferometry," Nature **365**(6448), 721–727 (1993).
8. J. Y. Finer, R. M. Simmons, and J. A. Spudich, "Single myosin molecule mechanics: piconewton forces and nanometre steps," Nature **368**(6467), 113–119 (1994).
9. F. E. Molloy, J. E. Bures, J. Kendrick-Jones, R. T. Tregear, and D. C. S. White, "Movement and force produced by a single myosin head," Nature **378**(6553), 209–212 (1995).
10. T. T. Perkins, "Angstrom-precision optical traps and applications," Annu. Rev. Biophys. **43**(1), 279–302 (2014).
11. E. A. Abbondanzieri, W. J. Greenleaf, J. W. Shaevitz, R. Landick, and S. M. Block, "Direct observation of base-pair stepping by RNA polymerase," Nature **438**(7067), 460–465 (2005).
12. LightSail, "The Lanetary society," http://www.planetary.org/explore/profects/lightsail-solar-sailing. [Accessed 8 November 2020] (1980).
13. J. Bookless and C. Mclnnes, "Control of Lagrange point orbits using solar sail propulsion," Acta Astronaut. **62**(2-3), 159–176 (2008).
14. L. Johnson, M. Whorton, A. Heaton, R. Pinson, G. Laue, and C. Adams, "NanoSail-D: A solar sail demonstration mission," Acta Astronaut. **68**(5-6), 571–575 (2011).
15. L. Johnson, R. Young, N. Barnes, L. Friedman, V. Lappas, and C. McInnes, "Solar sails: technology and demonstration status," Int. J. Aeronautical & Space Sci. **13**(4), 421–427 (2012).
16. X. Wang, J. Song, J. Liu, and Z. L. Wang, "Direct-Current nanogenerator driven by ultrasonic waves," Science **316**(5821), 102–105 (2007).
17. Y. Qi, J. Kim, T. D. Nguyen, B. Lisko, P. K. Purohit, and M. C. McAlpine, "Enhanced piezoelectricity and stretchability in energy harvesting devices fabricated from buckled PZT ribbons," Nano Lett. **11**(3), 1331–1336 (2011).
18. H. S. Kim, J. -H. Kim, and J. Kim, "A review of piezoelectric energy harvesting based on vibration," Int. J. Precis. Eng. Man. **12**(6), 1129–1141 (2011).
19. J. Li, X. Zhou, G. Huang, and G. Hu, "Acoustic metamaterials capable of both sound insulation and energy harvesting," Smart Mater. Struct. **25**(4), 045013 (2016).
20. M. Safaei, H. A. Sodano, and S. R. Anton, "A review of power harvesting using piezoelectric materials: state-of-the-art a decade later," Smart Mater. Struct. **28**(11), 113001 (2019).

Optics EXPRESS

21. W. Guo, C. Tan, K. Shi, J. Li, X. -X. Wang, B. Sun, X. Huang, Y.-Z. Long, and P. Jiang, "Wireless piezoelectric device based on electrospun PVDF/$BaTiO_3$ NW nanocomposite fibers for human motion monitoring," Nanoscale **10**(37), 17751–17760 (2018).
22. C. Dagdeviren, B. D. Yang, Y. Su, P. L. Tran, P. Joe, E. Anderson, J. Xia, V. Doraiswamy, B. Dehdashti, X. Feng, B. Lu, R. Poston, Z. Khalpey, R. Ghaffan, Y. Huang, M. J. Slepian, and J. A. Rogers, "Conformal piezoelectric energy harvesting and storage from motions of the heart, lung, and diaphragm," Proc. Natl. Acad. Sci. **111**(5), 1927–1932 (2014).
23. K. -B. Kim, W. Jang, J. Y. Cho, S. B. Woo, D. H. Jeon, J. H. Ahn, S. D. Hong, H. Y. Koo, and T. H. Sung, "Transparent and flexible piezoelectric sensor for detecting human movement with a boron nitride nanosheet (BNNS)," Nano Energy **54**(1), 91–98 (2018).
24. L. H. Fang, S. I. S. Hassan, R. A. Rahim, M. Isa, and B. bin. Ismail, "Exploring piezoelectric for sound wave as energy harvester," Energy Procedia **105**(1), 459–466 (2017).
25. S. N. Cha, J. -S. Seo, S. M. Kim, H. J. Kim, Y. J. Park, S. -W. Kim, and J. M. Kim, "Sound-driven piezoelectric nanowire-based nanogenerators," Adv. Mater. **22**(42), 4726–4730 (2010).
26. J. Zhang, Z. Fang, C. Shu, J. Zhang, Q. Zhang, and C. Li, "A rotational piezoelectric energy harvester for efficient wind energy harvesting," Sensor Actuat. A: Phys. **262**(1), 123–129 (2017).
27. H. -B. Fang, J. -Q. Liu, Z. -Y. Xu, L. Dong, L. Wang, D. Chen, B. -C. Cai, and Y. Liu, "Fabrication and performance of MEMS-based piezoelectric power generator for vibration energy harvesting," Microelectronics **37**(11), 1280–1284 (2006).
28. J. Ryu, J. -E. Kang, Y. Zhou, S. -Y. Choi, W. -H. Yoon, D. -S. Park, J. -J. Choi, B. -D. Hahn, C. -W. Ahn, J. -W. Kim, Y. -D. Kim, S. Priya, S. Y. Lee, S. Jeong, and D. -Y. Jeong, "Ubiquitous magneto-mechano-electric generator," Energy Environ. Sci. **8**(8), 2402–2408 (2015).
29. C. K. Kyu, I. Kim, K. -I. Park, M. H. Oh, H. Paik, G. -T. Hwang, K. No, Y. S. Nam, and K. J. Lee, "Virus-directed design of a flexible $BaTiO_3$ nanogenerator," ACS Nano **7**(12), 11016–11025 (2013).
30. H. K. Kim and Y. J. Kim, "High performance flexible piezoelectric pressure sensor based on CNTs-doped 0-3 ceramic-epoxy nanocomposites," Mater. Design **151**(1), 133–140 (2018).
31. M. Lee, C.-Y. Chen, S. Wang, S. N. Cha, Y. J. Park, J. M. Kim, L. -J. Chou, and Z. L. Wang, "A hybrid piezoelectric structure for wearable nanogenerators," Adv. Mater. **24**(13), 1759–1764 (2012).
32. B. Lu, Y. Chen, D. Ou, H. Chen, L. Diao, W. Zhang, J. Zheng, W. Ma, L. Sun, and C. Feng, "Ultra-flexible piezoelectric devices integrated with heart to harvest the biomechanical energy," Sci. Rep. **5**(1), 16065 (2015).
33. C. Dagdeviren, P. Joe, O.L. Tuzman, K. -I. Park, K. J. Lee, Y. Shi, Y. Huang, and J. A. Rogers, "Recent progress in flexible and stretchable piezoelectric devices for mechanical energy harvesting, sensing and actuation," Extreme Mach. Lett. **9**(1), 269–281 (2016).
34. I. Abdulhalim, "Coupling configurations between extended surface electromagnetic waves and localized surface plasmons for ultrahigh field enhancement," Nanophotonics **7**(12), 1891–1916 (2018).
35. A. Li, S. Isaacs, I. Abdulhalim, and S. Li, "Ultrahigh enhancement of electromagnetic fields by exciting localized with extended surface plasmons," J. Phys. Chem. C **119**(33), 19382–19389 (2015).
36. G. A. Farias and A. A. Maradudin, "Surface plasmons on a randomly rough surface," Phys. Rev. B **28**(10), 5675–5687 (1983).
37. Y. Fang and Y. Huang, "Electromagnetic field redistribution in hybridized plasmonic particle-film system," Appl. Phys. Lett. **102**(15), 153108 (2013).
38. K. Arya, Z. B. Su, and J. L. Birman, "Localization of the surface plasmon polariton caused by random roughness and its role in surface-enhanced optical phenomena," Phys. Rev. Lett. **54**(14), 1559–1562 (1985).
39. D. -H. Ha and J. -J. Kim, "Surface-enhanced raman scattering of the pyridine KCI-water-copper system: Temperature dependence," Phys. Rev. B **38**(17), 12704–12707 (1988).
40. M. Abutoama, S. Li, and I. Abdulhalim, "Widening the spectral range of ultrahigh field enhancement by efficient coupling of localized to extended plasmons and cavity resonances in grating geometry," J. Phys. Chem. C **121**(49), 27612–27623 (2017).
41. M. Abutoama, A. Bajaj, D. Li, Y. Wang, L. Jiang, and I. Abdulhalim, "Resonant modes of reflecting gratings engineered for multimodal sensing," APL Photonics **5**(7), 076108 (2020).
42. M. Abutoama, S. Isaacs, M. Ney, L. Zhong, D. Li, L. Jiang, and I. Abdulhalim, "Ultrahigh field enhancement optimization versus Rabi splitting investigated using au nano-bipyramids on metal film," J. Phys. Chem. C **123**(20), 12984–12996 (2019).
43. W. K. Liang, D. Li, Y. H. Sun, Z. Y. Li, L. Zhong, J. C. Zhang, Z. Q. Liang, I. Abdulhalim, and L. Jiang, "Growing in-plane multiplex plasmonic arrays for synergistic enhanced photocurrent response," Adv. Mater. Interfaces **7**(2), 1900966 (2020).
44. A. I. Hochbaum, R. Chen, R. D. Delgado, W. Liang, E. C. Garnett, M. Najarian, A. Majumdar, and P. Yang, "Enhanced thermoelectric performance of rough silicon nanowires," Nature **451**(7175), 163–167 (2008).
45. V. Annapureddy, H. Y. Lee, W. -H. Yoon, H. -J. Woo, J. -H. Lee, H. Palneedi, H. -J. Kim, J. -J. Choi, D. -Y. Jeong, S. N. Yi, and J. Ryu, "Enhanced magnetic energy harvesting properties of magneto-mechano-electric generator by tailored geometry," Appl. Phys. Lett. **109**(9), 093901 (2016).
46. K. -W. Lim, M. Peddigari, C. H. Park, H. Y. Lee, Y. Min, J. -W. Kim, C. -W. Ahn, J. -J. Choi, B. -D. Hahn, J. -H. Choi, D. -S. Park, J. -K. Hong, J. -T. Yeom, W. -H. Yoon, J. Ryu, S. N. Yi, and G. -T. Hwang, "A high output

Optics EXPRESS

magneto-mechano-triboelectric generator enabled by accelerated water-soluble nano-bullets for powering a wireless indoor positioning system," Energy Environ. Sci. **12**(2), 666–674 (2019).
47. C. Tadokoro, A. Matsumoto, T. Nagamine, and S. Sasaki, "Piezoelectric power generation using friction-induced vibration," Smart Mater. Struct. **26**(6), 065012 (2017).
48. H. Y. Lee, M. S. Kwak, K. -W. Lim, H. S. Ahn, and S. N. Yi, "Fabrication and time-dependent analysis of micro-hole in GaAs(100) single crystal wafer using wet chemical etching method," Korean J. Mater. Res. **29**(3), 155–159 (2019).
49. H. Y. Lee, J. -Y. Noh, M. S. Kwak, K. -W. Lim, H. S. Ahn, J. -H. Ahn, S. N. Yi, and J. Ryu, "Fabrication of microholes in silicon wafers by using wet-chemical etching," New Phys. **68**(8), 834–838 (2018).
50. C. Awada, C. Dab, J. Zhang, and A. Ruediger, "Observation of propagating surface plasmon polaritons by using functionalized tip-enhanced Raman spectroscopy," J. Raman spectrosc. **51**(8), 1270–1277 (2020).
51. T. R. Jensen, M. D. Malinsky, C. L. Haynes, and R. P. V. Duyne, "Nanosphere lithography: tunable localized surface plasmon resonance spectra of silver nanoparticles," J. Phys. Chem. B **104**(45), 10549–10556 (2000).
52. D. H. Ha, S. Kim, Y. J. Yun, H. J. Park, W. S. Yun, and J. -H. Song, "Plasmon resonance changes of gold nanoparticle arrays upon modification," Nanotechnology **20**(8), 085204 (2009).
53. C. Langhammer, Z. Yuan, I. Zoric, and B. Kasemo, "Plasmonic properties of supported Pt and Pd nanostructures," Nano Lett. **6**(4), 833–838 (2006).